PERGAMON

Atmospheric Environment 37 (2003) 363–382

ATMOSPHERIC ENVIRONMENT

www.elsevier.com/locate/atmosenv

An inter-comparison exercise of mesoscale flow models applied to an ideal case simulation

P. Thunis[a], S. Galmarini[a,*], A. Martilli[b], A. Clappier[b], S. Andronopoulos[c], J. Bartzis[c], D. Vlachogiannis[c], K. De Ridder[d], N. Moussiopoulos[e], P. Sahm[e], R. Almbauer[f], P. Sturm[f], D. Oettl[f], S. Dierer[g], K.H. Schlünzen[g]

[a] *Environment Institute, Joint Research Center, Ispra I-21020, Italy*
[b] *LPAS-IGE-DGR, EPFL, 1015 Lausanne, Switzerland*
[c] *Environmental Research Laboratory, Institute of Nuclear Technology and Radiation Protection, NCSR "Demokritos", GR-15310 Aghia Paraskevi, Attiki, Greece*
[d] *Flemish Institute for Technological Research (Vito), Remote Sensing and Atmospheric Processes, Boeretang 200, B-2400 Mol, Belgium*
[e] *Laboratory of Heat Transfer and Environmental Engineering, Box 483, Aristotle University, GR-54006 Thessaloniki, Greece*
[f] *Technical University of Graz, Institute of Internal Combustion Engines and Thermodynamics, Inffeldgasse 25, 8010 Graz, Austria*
[g] *Meteorological Institute, Centre for Marine and Climate Research, University of Hamburg, Bundesstr. 55, 20146 Hamburg, Germany*

Received 12 April 2002; received in revised form 7 August 2002; accepted 16 October 2002

Abstract

An exercise is described aiming at the comparison of the results of seven mesoscale models used for the simulation of an ideal circulation case. The exercise foresees the simulation of the flow over an ideal sea–land interface including ideal topography in order to verify model deviations on a controlled case. All models involved use the same initial and boundary conditions, circulation and temperature forcings as well as grid resolution in the horizontal and simulate the circulation over a 24-h period of time. The model differences at start are reduced to the minimum by the case specification and consist mainly of the parameterisation and numerical formulation of the fundamental equations of the atmospheric flow. The exercise reveals that despite the reduction of the differences in the case configuration, the differences in model results are still remarkable. An ad hoc investigation using one model of the original seven identifies the treatment of the boundary conditions, the parameterisation of the horizontal diffusion and of the surface heat flux as the main cause for the model deviations. The analysis of ideal cases represents a revealing and interesting exercise to be performed after the validation of models against analytical solution but prior to the application to real cases.

Keywords: Mesoscale flow models; Inter-comparison; Ideal case study

1. Introduction

Model inter-comparison has long been recognised as an important step in the evaluation procedure of numerical models. It is even mentioned as one of the requirements that must be met before the credibility of simulations performed with a model can be established by the scientific community (Pielke, 1984). Although based on the same set of conservation equations, models differ by the level of approximation adopted in solving them (e.g. anelastic, incompressible, nonhydrostatic, etc.), but they also differ by their numerical schemes or by the choice of different parameterisations to treat physical processes (e.g. turbulent diffusion). It is therefore interesting to know the variability of model results based on different numerical approaches, sets of parameterisations, and approximations. When no

*Corresponding author.
E-mail address: stefano.galmarini@jrc.it (S. Galmarini).

1352-2310/02/$ - see front matter
PII: S1352-2310(02)00888-9

observations are used, model inter-comparison exercises of course will never ensure that realistic results are obtained, but they may help in isolating parts of the model that lead to major differences. A further understanding of those differences can be gained by theoretical analysis of the differences or by using measurement data for comparison. This helps to detect weak areas of the model or to better know the limits of applicability of a given set of equations. As a side-product, inter-comparison exercises often help in the identification of programming errors.

In most of the mesoscale-model inter-comparison exercises performed to date, measurements were used for model evaluation purposes. As is always the case, in such exercises, only a limited number of measurements are available to initialise a model as well as to evaluate the results. There is therefore some freedom on the choice of the initial and boundary conditions and this freedom is used to get as close agreement as possible to the available measurements used for validation purposes. Practically speaking, a series of "trial and error" simulations is carried out, tuning "free" parameters. In this case, natural and unavoidable calibration is thus operated and the competence of the model user becomes the key factor in determining the quality of the model results. Not only model results but also modeller skills are evaluated in those type of exercises.

The purpose of MESOCOM (MESOscale Model InterCOMparison) was to compare model results in the case of thermally forced circulation only, trying to reduce to the minimum the influence of the model user and at the same time to understand how far results of different approaches to mesoscale modelling can differ when applied to simple and controlled conditions. To this end, an ideal domain is built for which the sources of differences are reduced to the minimum. The case considered is therefore simple but for it no analytical solution is known. On the other hand, no experimental evidence is used to quantify the model success in reproducing the flow patterns, and model results can only be estimated on physical grounds. This helps in discarding some of the solutions, certainly not in defining a reference model.

The overall goal of this inter-comparison exercise is to determine the range of variability of different models when applied to a relatively simple situation and to provide an explanation to this variability. In Section 2, a description of the case set-up is given. Section 3 gives a short description of the participating models. Section 4 provides details on the methodology followed to compare the results. The main results of the inter-comparison are discussed in Section 5 whereas the main causes of variability among the models, identified in the frame of MESOCOM, are discussed in Section 6. Finally, conclusions are given in Section 7 and future perspectives in Section 8.

2. Description of the ideal simulation case

The choice of the domain configuration, and of the initial and boundary conditions to be used in MESOCOM was motivated by the following considerations:

(1) It should be simple enough to ease the understanding of the results and to allow for a relatively simple specification of the initial and boundary conditions.
(2) It should be complex enough to force participants to work in a "blind way", i.e. without referring to known solutions of almost similar cases.
(3) It should remain realistic enough without being too close to known existing geographical domains and atmospheric conditions.

According to those requirements, the selected domain of calculation is shown in Fig. 1. It is composed of a $50 \times 50\,\mathrm{km}^2$ domain containing two gaussian-shaped mountains of different altitude on the west side of the domain whereas a water area is located on the eastern side. Those two areas are separated by a north–south oriented coastline. Only two different land use soil types are included: water and land (water occupies the 16 most eastern grid cells on each E–W cross-section). Sea-surface temperature is kept constant at 293 K during the whole 24 h integral cycle whereas land surface temperature is governed by two sine functions that are characterised by a night time-cooling being half of the value of the day-time warming, i.e.:

$$\theta(z,t) = [293.16 + \Gamma z] + 15\,\sin(2\pi(t-6)/24) \quad \text{(from 0600 to 1800 LST)},$$

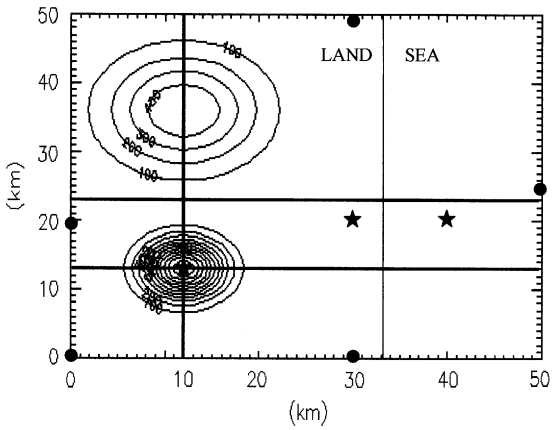

Fig. 1. Geographical set-up of the Mesocom domain including topography and two distinct land uses. Stars indicate the locations at which time evolution of different parameters at surface and 2700 m have been performed. Horizontal lines are indicative of the locations where cross-sections have been analysed and circles are the studied boundary locations.

$$\theta(z,t) = [293.16 + \Gamma z] + 7.5\sin(2\pi(t-6)/24) \quad \text{(from 1800 to 0600 LST)},$$

where θ is the surface potential temperature, Γ the temperature lapse rate and z the altitude above sea level. The land surface roughness length was fixed to 0.1 m. No specific value has been imposed for the sea-surface roughness length.

Horizontally, the grid contains 50×50 cells with a uniform 1 km resolution. Vertically, the proposed grid for those who use terrain following coordinate systems is stretched (factor of 1.2) and 22 levels are used up to 5000 m with the first level located at 30 m: 0, 30, 66, 109, 161, 223, 298, 387, 495, 624, 779, 965, 1187, 1455, 1776, 2191, 2623, 3123, 3623, 4123, 4623, 5123 m. For other co-ordinate transformations (e.g. Cartesian, pressure, etc.), the choice of the vertical grid is left to the modeller.

Boundary conditions (BC) on transport are fixed in a comparable way in all models in order to achieve a meaningful inter-comparison of the results on a relatively limited area such those chosen in MESOCOM. The BCs for wind and temperature transports are fixed for inflow only. Boundary conditions for terms like the horizontal diffusions are left free, since their influence on model results will significantly affect the results. The value of those BC are imposed as follows: once three-dimensional wind and temperature fields are obtained from the initialisation procedure (from the profiles described below), the values of wind and temperature at the boundaries are then set to those initial values and kept constant during the whole simulation. Clearly, these conditions are not realistic ones but as mentioned above, this inter-comparison exercise is aiming at an idealised case and the BC were fixed according to criteria of simplicity and extensive application to all participating models.

The simulation starts at 1800 LST and lasts for 30 h but only the results from 0000 to 2400 LST are considered for comparison. The first 6 simulation hours were used, however, to check that all models correctly set the initial and boundary conditions. The fictitious domain is located at 45°N. The initialisation procedure is based on a single profile initialisation. The synoptic wind is assumed to be 1 m/s from West and the vertical profile obtained at a sea-level location shows a constant 1 m/s value down to 2000 m and then a linear decrease to reach zero at surface. For potential temperature, a 3 K/km stable gradient is assumed everywhere (i.e. potential temperature is constant on horizontal planes). The boundary conditions at the model top are the top value of the prescribed profiles which are kept constant throughout the simulation period. Both the short and long wave radiation divergence terms are omitted in the energy conservation equation for these comparisons to avoid as much as possible differences due to parameterisations.

Each modeller was asked to provide hourly 3-D data including wind, temperature and surface heat flux values with a time resolution of 1 h.

3. Participating numerical models

Six numerical mesoscale models participated in the MESOCOM exercise. These models are listed below:

- The MEsoscale MOdel (MEMO)
- The GRAz Mesoscale Model (GRAMM, Oettl, 2000; Oettl et al., 2000)
- The MEsoskaliges Chemie, TRAnsport- und Strömungsmodell (METRAS, Schlünzen, 1990; Schlünzen et al., 1996)
- The Finite Volume Model (FVM, Clappier et al., 1996)
- The Advanced Regional Prediction System (ARPS, Xue et al., 2000a, b)
- The ADREA mesoscale model (Bartzis, 1989; Bartzis et al., 1991)

In addition to those six models, the Topography Vorticity Model (Thunis and Clappier, 2000; Schayes et al., 1996) was used by the Joint Research Centre to set up the case and the inter-comparison methodology. As such, it should be noted that this model did not exactly follow the same "blind" procedure as imposed to other models. This means that this model was used for the preliminary set up of the case study and its results were produced once the other model's results were submitted to the evaluation. All models are nonhydrostatic. Models are either based on the compressible (ARPS, ADREA), or anelastic (MEMO, METRAS, GRAMM, FVM and TVM) approximation of the mass conservation equation. The vertical coordinate system is terrain following (σ_z) for all models except for ADREA which is built in a Cartesian coordinate system. Models do exhibit a large variability in their numerical techniques. Models like MEMO or ARPS are finite-difference models whereas FVM is partly based on finite-element and partly on finite-volumes techniques. As can be seen from Table 1 that summarises the characteristics of the participating models, these seven models use a wide range of approximations to the basic set of conservation equations and varied numerical schemes and parameterisations.

4. Methodology of the inter-comparison

In order to make the results comparable and independent of the different types of coordinate system

Table 1

Model	Eq. set	Advection scheme	Turbulence scheme	Discretization	Horiz. diffusion
MEMO	NH-A	TVD scheme			
GRAMM	NH-A	Time: Adams-bashfort Spatial: TVD	1.5-order TKE	FV. Hexa-hedronal grid	Prop. to Horiz and vert grid and to Vert Exchange coefficients
FVM	NH-C	3rd order PPM	Bougeault and Lacarrere	Control volume finite element	Proportional to the horizontal mesh size multiplied by the square root of the turbulent kinetic energy
METRAS	NH-A	Momentum eq: time: Adams-Bashforth Space: centred scalar quantities: time: forward, space: upstream in space (mesoscale perturbation), centred: large scale perturbation	Stable, neutral: mixing length approach unstable: counter-gradient scheme of Lüpkes and Schlünzen, (1996)	FD-FV	No explicit Horiz diffusion calculated. Seven-point filtering for wind field, numerical diffusion for temperature and humidity field via upstream scheme
ARPS	NH-C	CTCS with 4th order accuracy in space	1.5-order TKE	FD	Proportional to the horiz. mesh size multiplied by $(TKE)^{1/2}$ (TKE-l model). Additionaly: 4th order numerical smoothing
ADREA	NH-C	Upwind	1 equation TKE-l model	FV, Cartesian with surface and volumes porosities to account for irregular geometries	TKE-l model where l is 3-D. Diffusivity depends on the horizontal length scale (function of the distance from obstacles).
TVM	NH-A	3rd order PPM	1.5 TKE	FD-FV	Constant ($300\,m/s^2$)

CTCS: Centred in space, centred in time; FD, FV: Finite differences, finite volumes; NH, H: Nonhydrostatic, hydrostatic; A,C,I: Anelastic, compressible, incompressible; PPM, TVD: Piecewise Parabolic Method, total variational diminishing scheme; TKE: Turbulent kinetic energy

used by the participants, outputs were requested on an independent grid. Results had to be interpolated to "true" terrain following coordinate isolines, the choice of the interpolation technique being left to the participating modellers. The information requested includes wind (Cartesian components), potential temperature (in K) and surface heat fluxes (W/m^2). Each participating modelling group provided these fields on an hourly basis for the whole domain points matrix and for the whole 30 h integration cycle.

This large amount of data did not allow an exhaustive analysis of the differences between the model results. Consequently, it was decided to define a multi-step procedure that would enable us to (1) check the correct setting of the requested boundary and initial conditions and (2) evaluate the model differences for selected aspects.

The adopted procedure included the following sequential steps:

(0) verification of mass conservation;
(1) comparison of time series of surface potential temperature and wind data at three different locations throughout the domain (see Fig. 1) (mountain, flat land, and sea);
(2) comparison of the elevated grid level potential temperature and wind field at three locations for all hours;
(3) comparison of vertical profiles of potential temperature and wind at five boundary locations at a given time (see Fig. 1);
(4) comparison of two horizontal East–West profiles of potential temperature and wind at the first vertical level at three given times (see Fig. 1);

(5) comparison of one horizontal North–South profiles of potential temperature and wind at the first vertical level at three given times (see Fig. 1);
(6) comparison of the 24 h cycle (from 0000 to 2400 LST) of the first vertical level 2-D wind field;
(7) comparison of the 24 h cycle (from 0000 to 2400 LST) of the first vertical level 2-D temperature field;
(8) comparison of North–South cross section for vertical velocity at three given times (see Fig. 1);
(9) time evolution of standard deviation and root-square error at five different height levels for five different times;
(10) comparison of surface heat fluxes at eight different times;
(11) check of initial discrepancies in the first hours of simulation and their subsequent propagation.

As mentioned earlier, the succession of these steps, particularly step 0–3, was designed to check whether or not a model was using the prescribed boundary and initial conditions. Fulfilment of steps 0 and 1 were in fact considered as a fundamental requirement in order to consider further comparison steps. A discussion of the main model differences will now be given for each of those steps.

5. Discussion of the results

As mentioned above, step 1 was performed to make sure that each participant imposed the correct surface temperature forcing, a prerequisite for a further comparison of the results. An additional test has been performed to check the initial 3-D fields. These fields have gone through the series of steps described above to identify possible discrepancies in the setting of initial conditions. This was considered important as the space-time scale and the geographical set-up of the case discussed in the previous section are such to generate dominant mesoscale thermally driven circulations, directly driven by the surface boundary conditions. Steps 0 and 1 were successfully achieved by all participants no results will therefore be presented since they are not worth of notice and only a discussion of the following steps is given hereafter.

5.1. STEP (2): Top level fields

Two different locations within the domain (refer to Fig. 1) were used to compare the time evolution of wind and temperature fields at a height of 2700 m above ground level (a.g.l.). Fig. 2 shows the behaviour of potential temperature and wind speed at the above-sea location (see Fig. 1). All models exhibit a relatively constant temperature throughout the day except for ARPS and METRAS that exhibit some warming during the afternoon (excess of 2° compared to other models). This feature is also found over flat land (not shown) but at the mountain location (not shown), only METRAS shows an extra warming compared to other models.

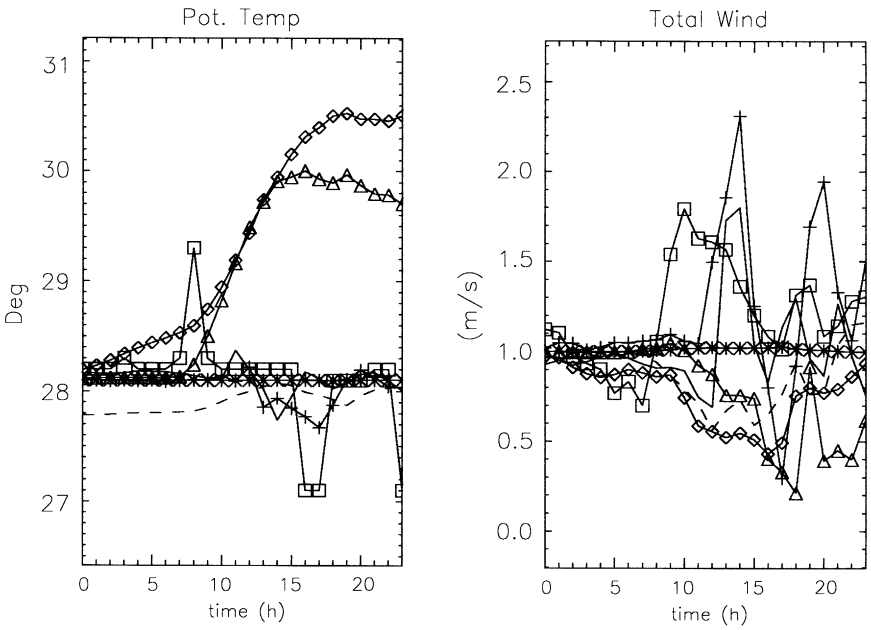

Fig. 2. Temporal profile of the potential temperature and total horizontal wind fields at 2700 m and grid location (40, 20). The line symbols valid also for all following figures are: solid line (model 00-TVM), dotted line (model 01-MEMO), asterisk-line (model 04-GRAMM), plus-sign line (model 05-FVM), diamond-line (model 07-METRAS), triangle line (model 08-ARPS) and square-line (model 11-ADREA).

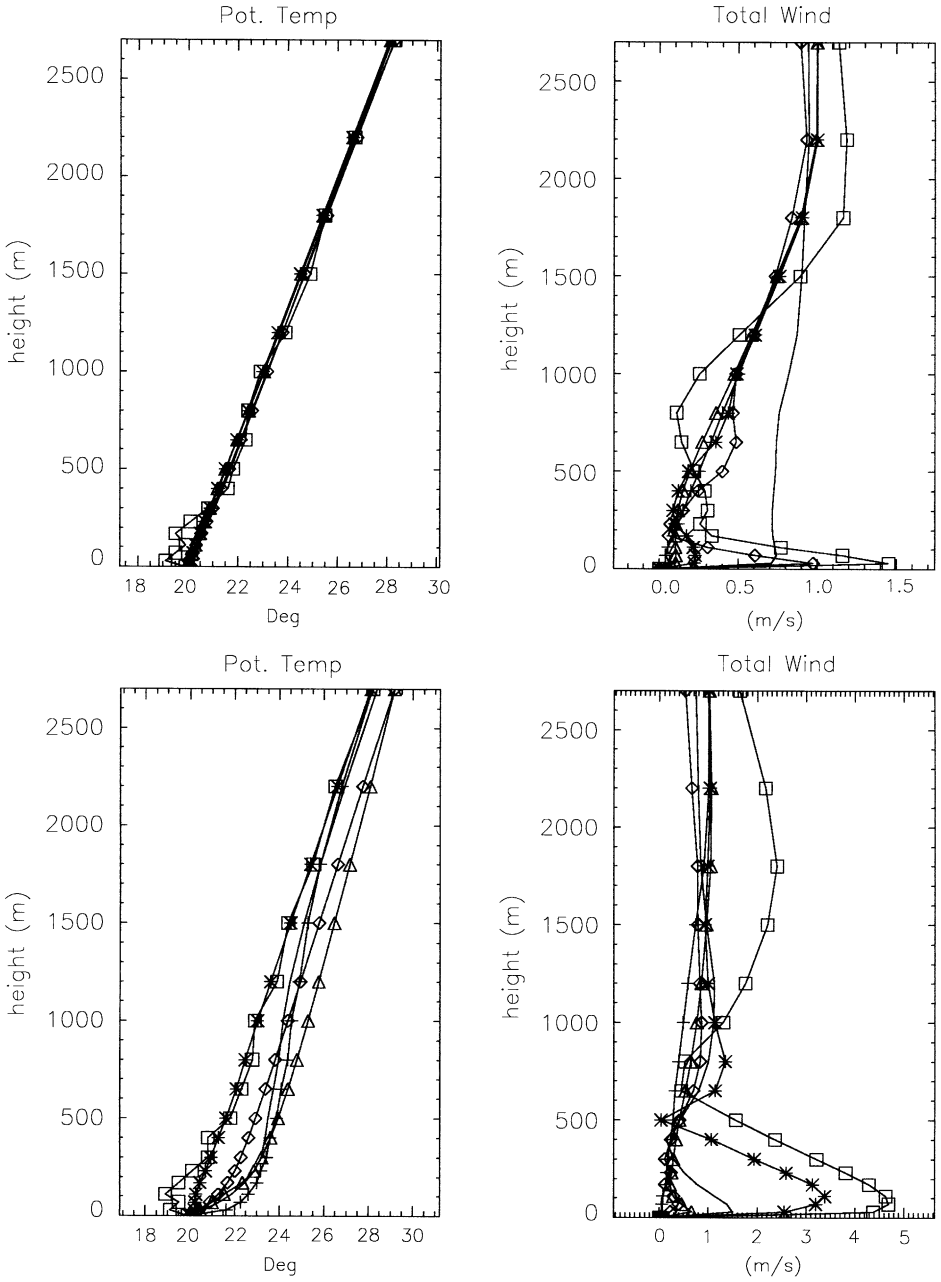

Fig. 3. (a) Vertical profile of potential temperature and wind field at the Eastern boundary at 0300 LST. See Fig. 2 for explanations of the line codes. (b) Same as Fig. 3a but at 12:00.

The horizontal wind field comparison over the sea location (Fig. 2) shows that all models predict the initial wind value during the night time period but it also shows that predicted wind fields, even though they are far from the surface, exhibit relatively large variations (difference of about 2 m/s between model METRAS and FVM at 1400 LST). Note that this behaviour is similar over the flat land and mountain locations although the differences are not so marked over the latter one. In summary, it appears that when the orographic forcing becomes more important, models are forced to behave in a more coherent way.

5.2. Step (3): Boundary vertical profiles

The Eastern boundary vertical profiles show very similar temperature profiles at 0300 LST (Fig. 3a) except in the first few hundreds of metres where differences in

the cooling rate exist. Model ADREA shows about 2 K lower temperatures than other models near the surface. The wind profile at the same time shows differences near the surface for some models. TVM shows differences within the first 200 m. This could be connected to the implementation of the BC in terms of vorticity. At 1200 LST (Fig. 3b), differences are still present in the wind field profile but the temperature now also exhibits relatively large differences at heights reaching up to 2500 m as already seen in Fig. 2. Differences in the wind field remain of the same order of magnitude as during night-time whereas they amplify for temperature. The same behaviour is observed at other boundaries. Note that the wind fields being relatively weak, these differences are not really significant, exception made for ADREA and GRAMM which produces winds of about 3–4 m/s. Temperature differences appear at high altitudes both at the Eastern and Western (not shown) boundaries, this is either a problem of boundary conditions, or of energy conservation or of parameterisations implicitly included in some of the models and not in others. This observation is in agreement with the time evolution warming at the top of the model discussed above for ARPS and METRAS.

5.3. Step(4) East–West (x–z) near surface profiles

At 0300 LST, the E–W profile (Fig. 4) passing through the plain (see Fig. 1) shows different temperature cooling among the models. Some models (e.g. ADREA and METRAS) exhibit a clear cooling about 3° whereas other models like TVM (Fig. 4) keep unchanged temperatures. Since the parameterisation of long wave radiation has been switched off for all models, these differences are either due to boundary conditions or to differences in the parameterisation of the surface layer. As expected, all models converge towards the same temperature over sea except for ADREA which exhibits a 1° difference, which could be due to different roughness lengths imposed over the sea-surface. Wind speeds at that time, are relatively low but differences exist between models which predict very low wind speeds such as MEMO and models that predict marked variations like TVM or ADREA. It is interesting to note that for x ranging between 10 and 15, and $y = 23$ as in Fig. 4 (the valley between the two hills), some models show a maximum in wind speed (TVM, ADREA, FVM) while other models show a minimum (GRAMM, ARPS and METRAS). It seems that the first group sees an acceleration in the mountain gap whereas the second group does not. For this latter group, the minimum is probably linked to the convergence of the slope flows from the two mountains. The section passing above the mountain ridge (Fig. 5) is interesting in that it shows that the temperature cooling variability is well marked only over flat land. Indeed, temperature predicted at the top of the 1200 m high mountain are very similar whereas over flat terrain, the disagreement reaches 4° among models. The differences result from the additional transport from the mountains towards the plain by katabatic flows. Wind speeds are relatively low (between 0 and 1 m/s) and show a larger variability in their N–S component than in their E–W one.

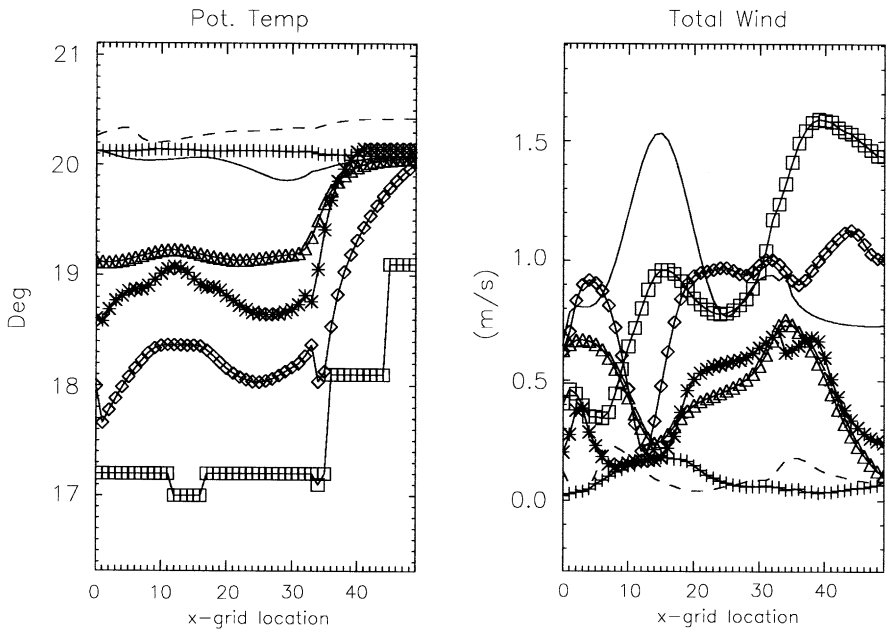

Fig. 4. Potential temperature and wind field XZ section passing through the hills ($Y = 23$) at 03:00 LST.

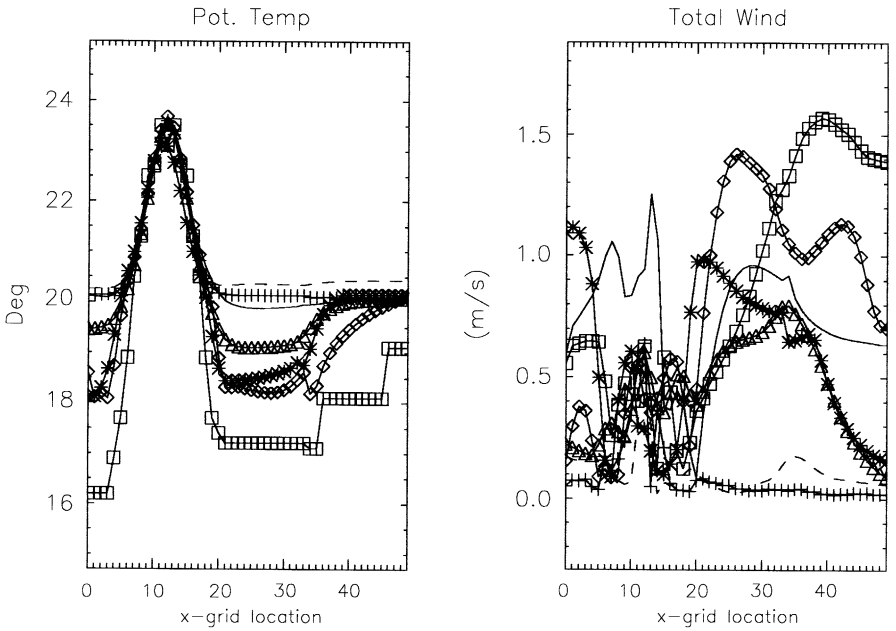

Fig. 5. Same as Fig. 4 but for a XZ section passing through the mountain ridge ($Y = 12$).

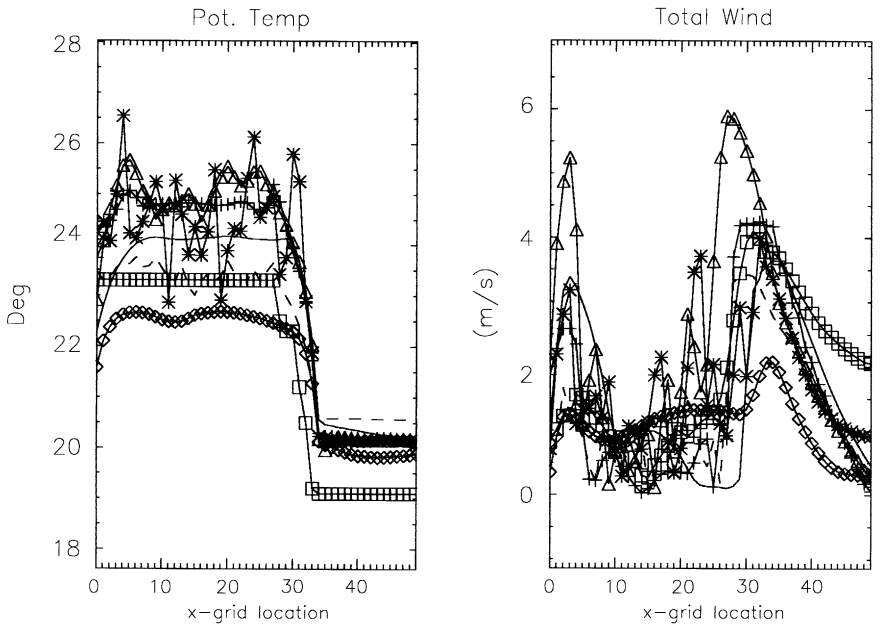

Fig. 6. Same as Fig. 4 but at 10:00 LST.

At 1000 LST (Fig. 6), the E–W plain profile shows that warming has now taken place. Once again, differences exist in the value of this warming (variability of about 3°). This warming has led to the development of a sea-breeze circulation from which the velocity peak is visible. All models predict a sea-breeze intensity of about 4 m/s located at grid point 30–32 with two exceptions being ARPS that predict a much stronger sea-breeze of 6 m/s further inland (grid point 27) and METRAS that predict a slighter sea-breeze of 2 m/s still

further offshore (grid point 35). Note that these two models are the ones that predicted the larger and smaller differential heating between land and sea, respectively.

The mountain profile (Fig. 7) illustrates the same characteristics. On these sections, one can isolate two peaks corresponding to the sea breeze and slope winds circulations. One can see that the variability of the resulting wind fields is much larger for slope winds than for sea breeze. The models predicting the largest sea-breeze peak are also the ones to give the stronger slope winds. Some models also predict a breeze entering from the western side of the domain, the corresponding peak being merged with the up-slope western circulation one.

At 1200 LST (Figs. 8 and 9), the EW plain and mountain profiles both illustrate the same characteristics than at 1000 LST but emphasising them. Indeed, the sea-breeze peak still appear but with different intensities and locations, from grid point 20 with 7 m/s for ARPS to grid point 35 and 3 m/s for METRAS). The variability in the wind velocities in between the two mountains is quite large with models speeds ranging from 2 to 6 m/s.

The mountain profile shows a temperature variability that reaches 4–5° over land whereas all models converge towards the same temperature over the sea (except ADREA 1° less). The total wind shows a relatively similar behaviour for the sea-breeze part (from grid point 25 to 50) whereas the variability is large (from wind speeds of 3 m/s [GRAMM] to—6 m/s [ARPS]) in between the sea-breeze front and the mountain ridge (from 25 to 15). On the mountain, the forcing being well defined, all models again converge towards more similar values although a variability of a factor of 2 is observed in this region (from grid point 0 to 10).

5.4. Step (5): South–North near surface profiles

At 0300 LST (not shown), as discussed above, the temperature cooling is again showing differences over flat land whereas temperature at mountain sites are similar. The wind field shows some variability but all values are below 1 m/s. At 1000 LST (Fig. 10), the predicted temperature ranges from 24 to 27 except for GRAMM, which hits 30°. The u and v wind fields show a similar pattern for all models, putting in evidence the slope winds. It is interesting to note, however, that some models predict very low slope winds of about 1 m/s (ADREA) compared to others that predict 7 m/s (GRAMM). This coincides with the extra warming observed by this model (see fluxes interpretation in section below).

5.5. Step (6): Near-surface 2-D wind fields

At 0300 LST (Fig. 11), the wind field predicted by all models remain relatively weak (maximum intensities range from 0.62 m/s for MEMO to 2.09 m/s for TVM). No well-defined structure appears except for down-slope winds or mountain deflection, which are well present in some simulations (e.g. TVM, GRAMM) and absent in others (e.g. MEMO, FVM).

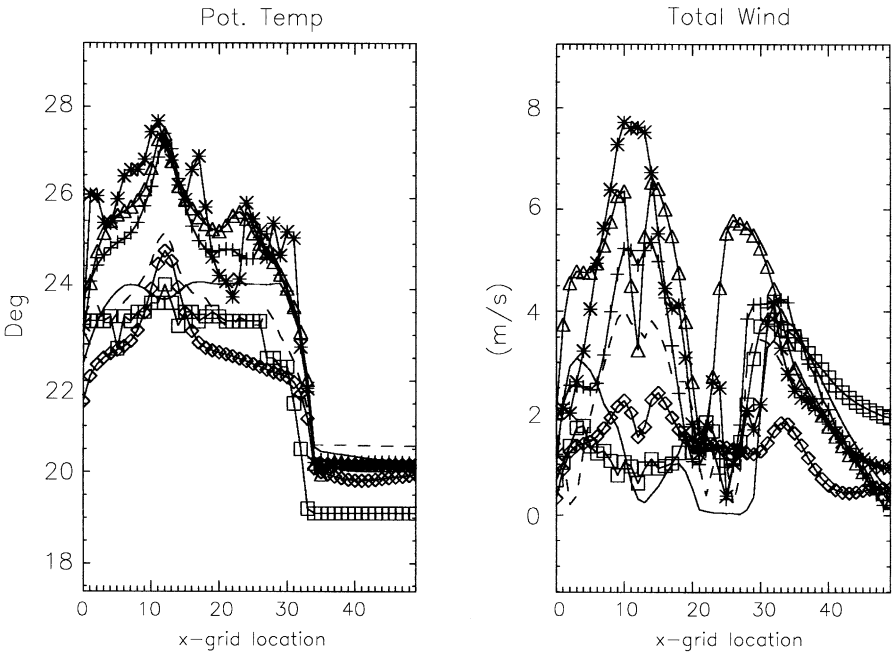

Fig. 7. Same as Fig. 5 but at 10:00 LST.

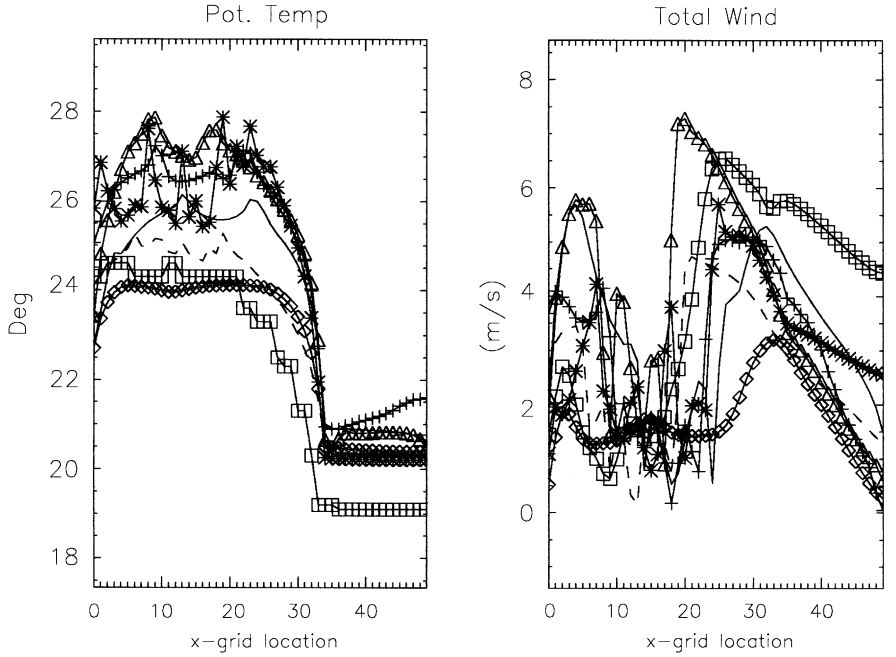

Fig. 8. Same as Fig. 6 but at 12:00 LST.

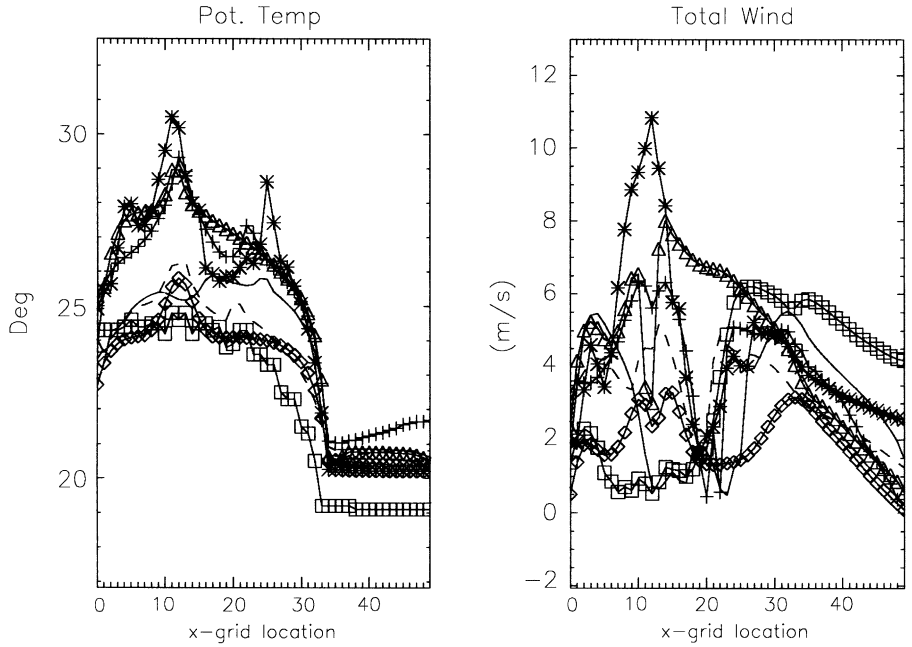

Fig. 9. Same as Fig. 7 but at 12:00 LST.

At 0900 LST (Fig. 12), a well-defined sea-breeze front is predicted by all models except for METRAS that predict a relatively smooth wind field all over the domain with intensity smaller than other models (1.8 m/s). Indeed, most models show a sea-breeze front located at about grid point 30 with an intensity ranging from 2.5 to 5 m/s, the most intense sea-breeze penetrating further inland. The prediction of up-slope winds is on the

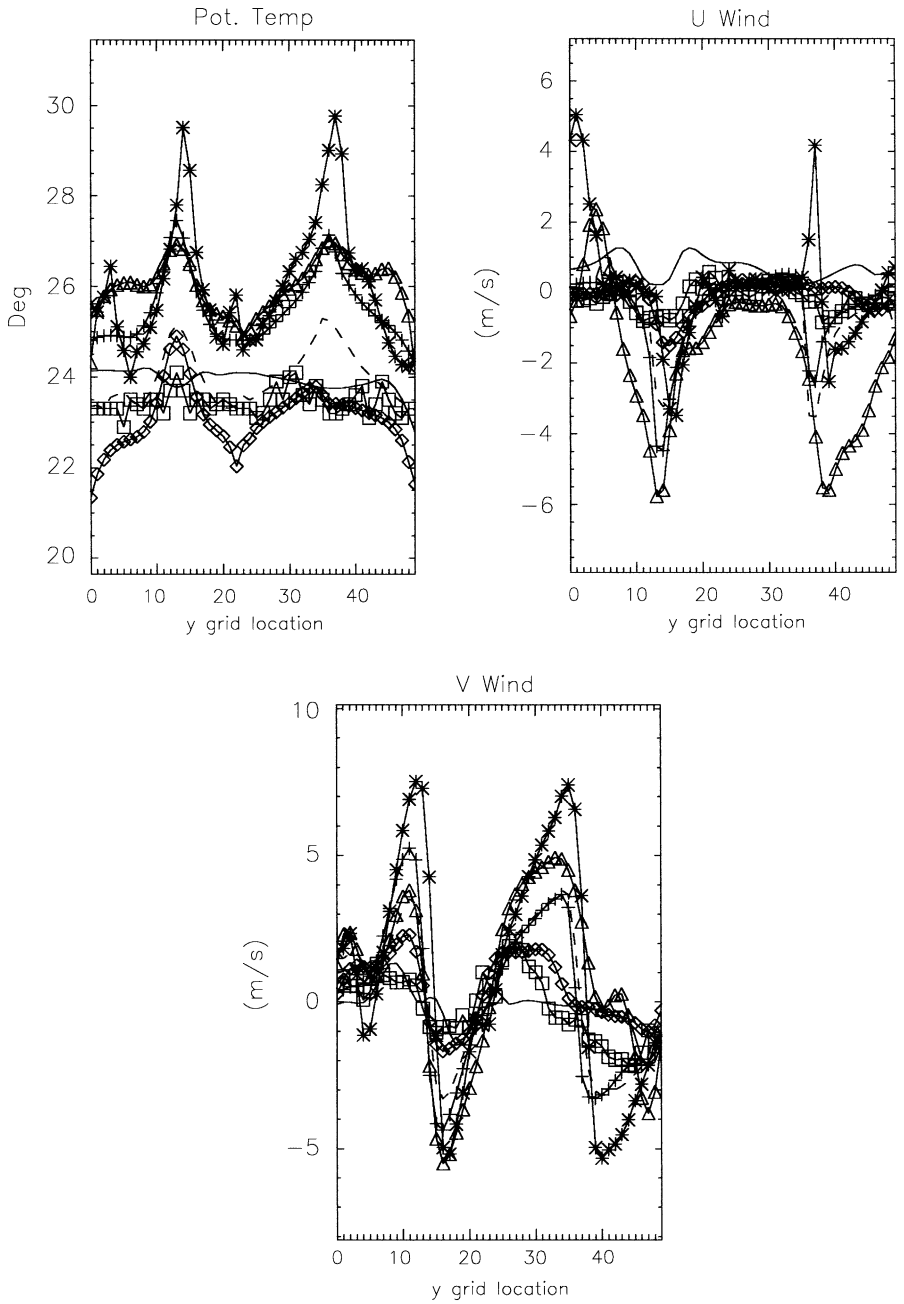

Fig. 10. Potential temperature, East–West and North–South wind components along a *YZ* section passing through the two mountain ridges at 10:00 LST.

contrary extremely different from one model to the other. GRAMM predicts slope winds of about 7 m/s whereas FVM modelled up-slope winds are limited to 3 m/s. It is interesting to note, however, that these two models predict similar sea-breeze intensities (about 3 m/s). This could indicate a difference in the formulation of horizontal diffusion over sloped terrain between the two models or in the way in which mesh deformations are numerically treated and its consequent impact on pressure gradient computation. On the Eastern side of the domain as well as at the Northern and southern sides, well-developed breezes are also simulated in all

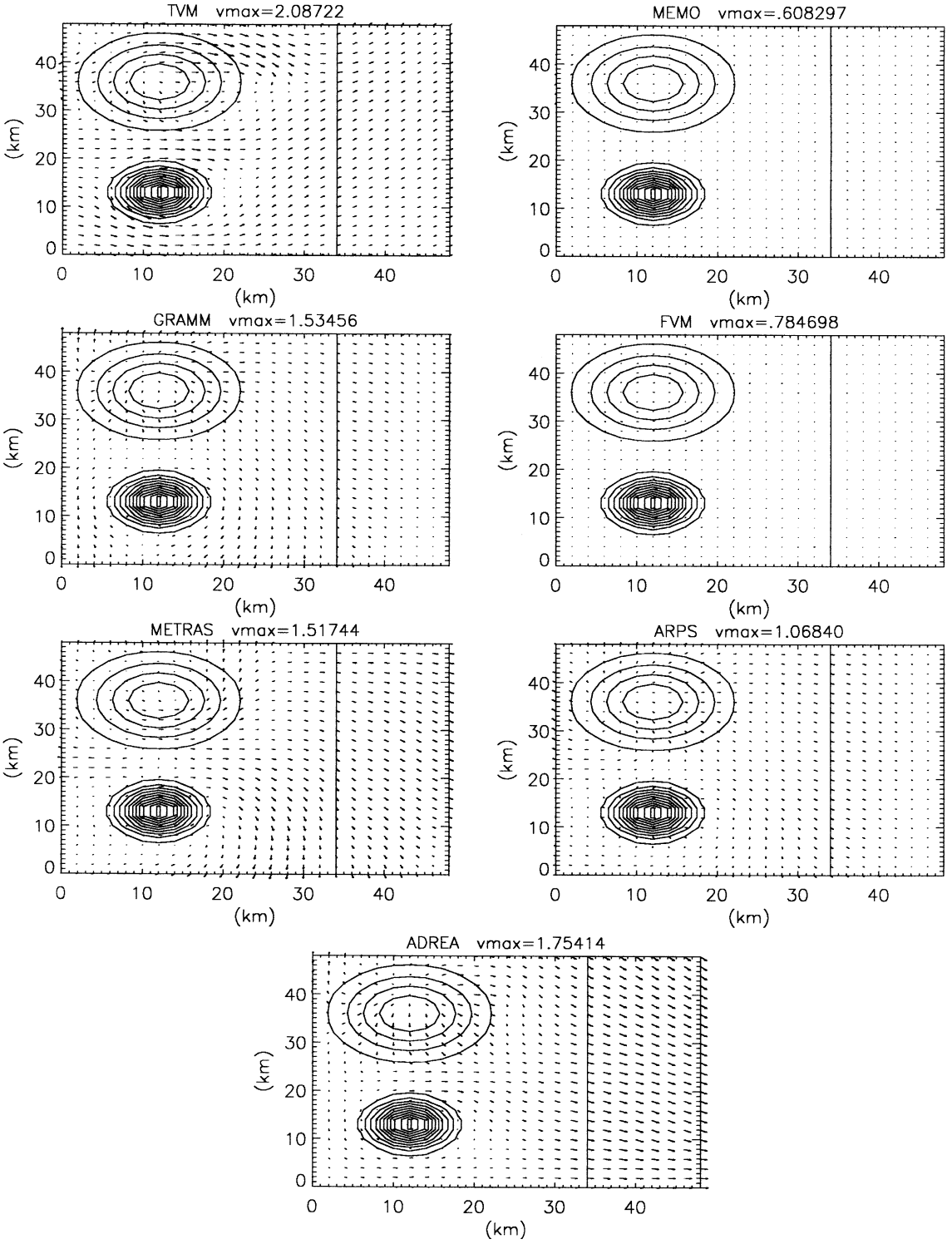

Fig. 11. Comparison of the surface wind fields at 03:00 LST. For clarity, only one arrow on two has been plotted.

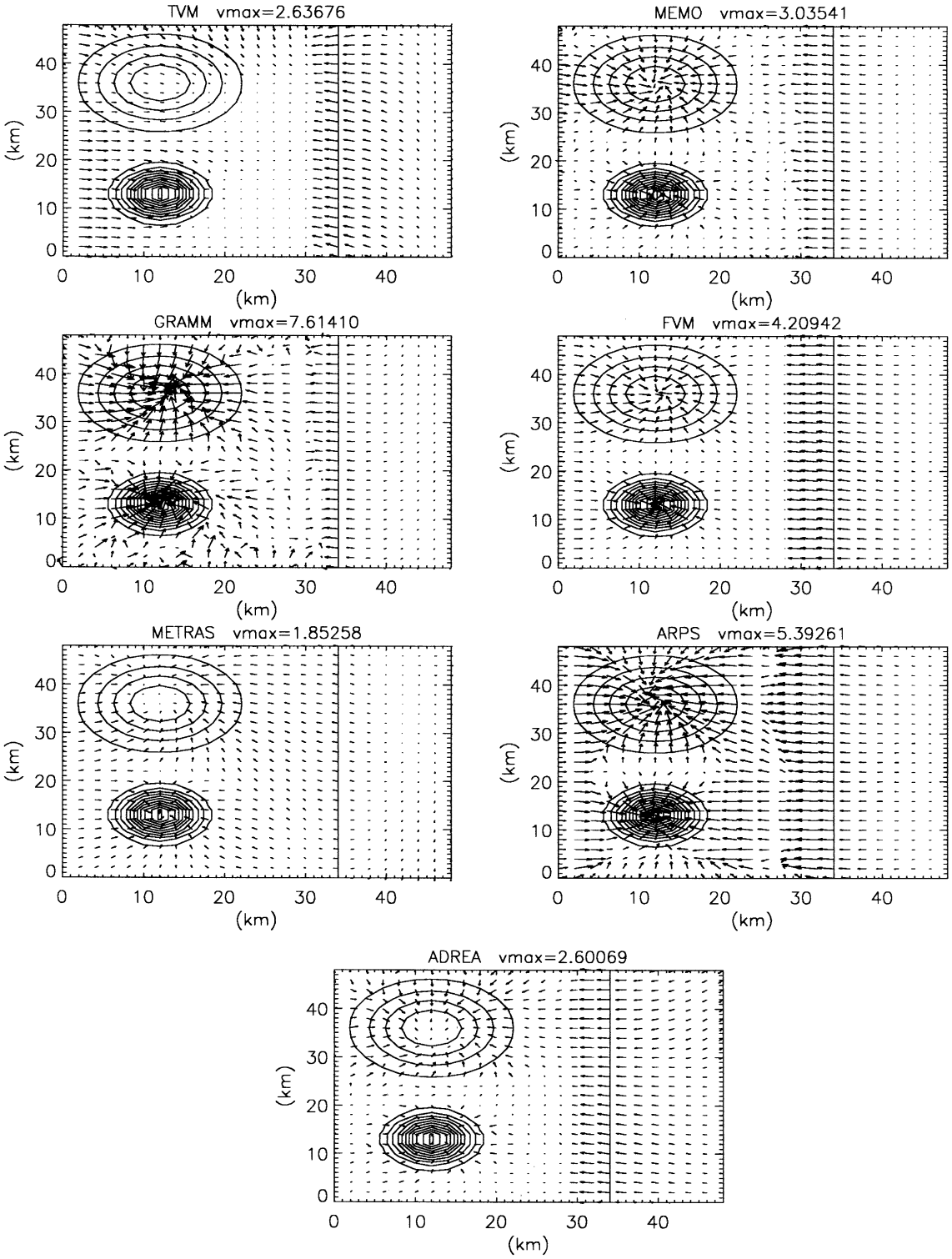

Fig. 12. Comparison of the surface wind fields at 09:00 LST.

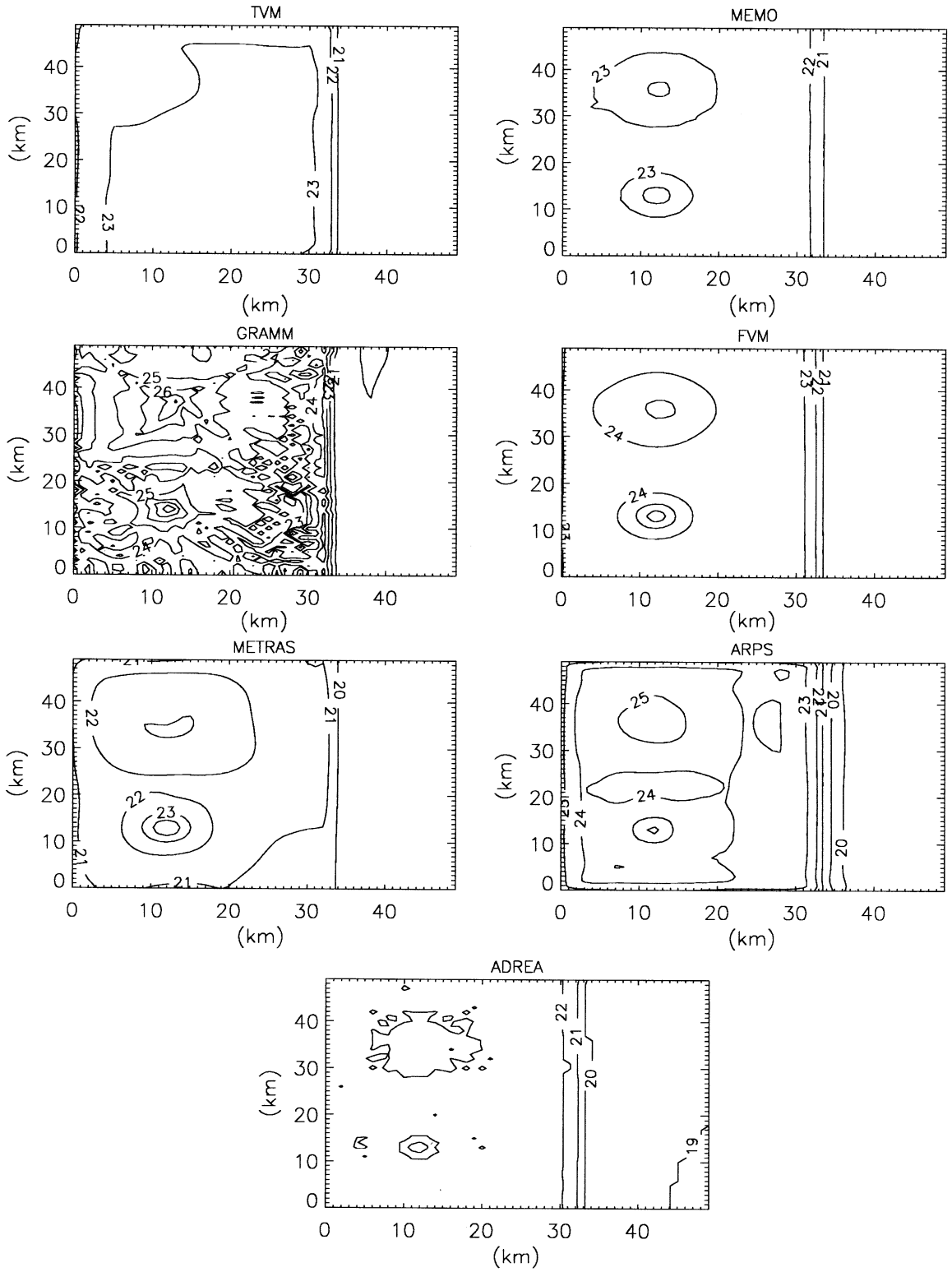

Fig. 13. Comparison of the first level potential temperature at 09:00 LST.

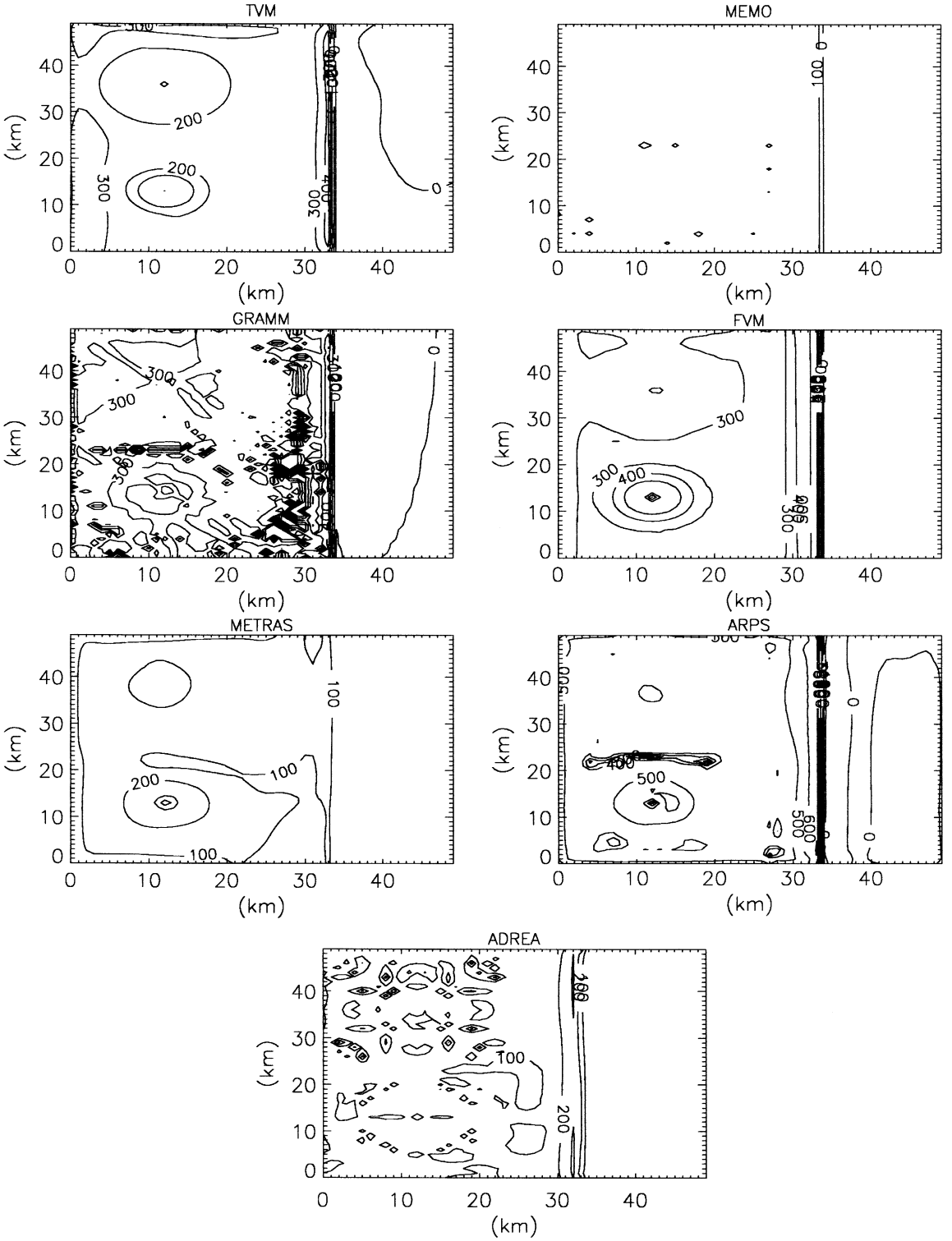

Fig. 14. Comparison of the sensible heat flux at 09:00 LST.

model results but they differ significantly in their amplitude. This seems to indicate the presence of differences in the treatment of inflow boundary conditions although they should have been fixed similarly for each model. Other explanations for the different intensities of the land-sea breeze circulations are the differences in the land–sea temperature contrast due to the different turbulence parameterisations. Note also that large differences appear in the area located in between the sea-breeze fronts, where more or less organised wind field structures appear. One important factor that leads to these differences is probably the horizontal diffusion parameterisation, which is treated in different ways by the models participating in this study (refer to Table 1). After 1200 LST (not shown), differences among models continue to increase and become at those times difficult to intercompare.

5.6. Step (7): Near-surface 2-D temperature fields and surface fluxes

At 0300 LST (not shown), all temperature fields are pretty similar for all models, except for the extra-cooling observed for some models over the plain (e.g. ADREA). At 0900 LST and 1200 LST (only 0900 LST is shown in Fig. 13), the extra-warming is well marked for some models. Note that the two models that cool more than others during the night (ADREA and METRAS) are also the one to warm the less during daytime. Responsible for those differences is the sensible heat flux (Fig. 14) that exhibits differences reaching a factor 3

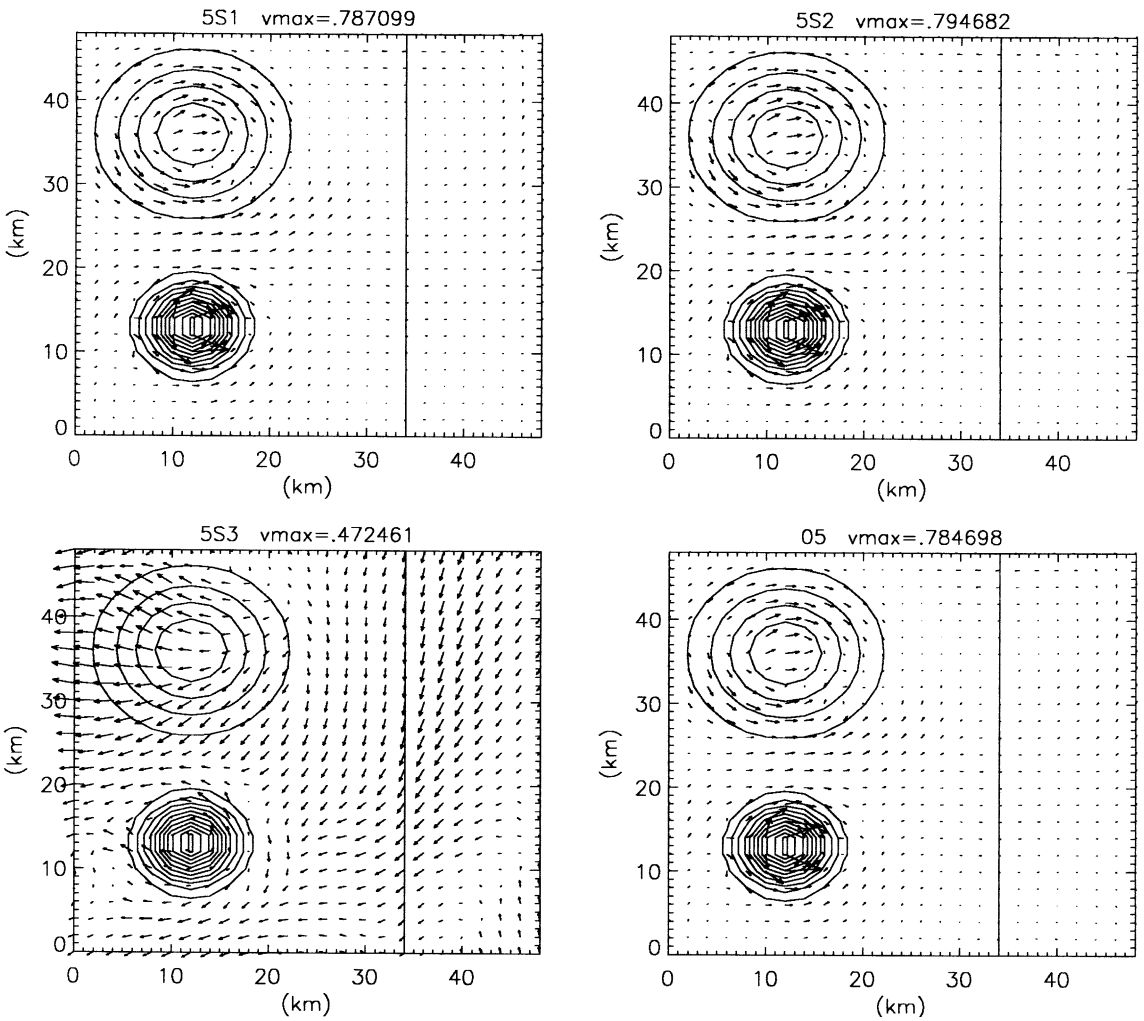

Fig. 15. Comparison surface wind field at 03:00 LST for a simulation obtained (1) with no horizontal diffusion (S1 upper left), (2) with horizontal zero-gradient BC on temperature (S2, upper right), (3) with horizontal zero gradient BC for temperature and wind (S3, lower left) and (4) base case simulation (corresponding to MOD05 in previous graphs (lower right). MOD05 is FVM.

or 4 at 0900 LST. These differences point out the importance of the surface flux parameterisation in the prediction of near surface temperature and wind fields.

6. Reasons for differences

Considering the results described above, quite a large variability arises between the fields predicted by the different models. In this section, it is intended to quantify the variability between results obtained with different configurations of the same model. Two factors thought to be of prime importance in explaining the variability of the results will be explored. These are the setting of boundary conditions and the value of the horizontal smoother. Although the first of these factors (boundary conditions) had been fixed for each participating model, the diversity of the model formulations and numerical schemes made it difficult to ensure a proper setting of the imposed conditions. For what concerns the second factor (horizontal smoother), no imposed value has been fixed, so that the participants have followed different approaches (see Table 1). Note that those two factors have been raised as main contributors in explaining the variability in other intercomparison exercises (Doyle et al., 2000).

A quantification of the variability obtained with one model is here performed, using FVM results as base case (S0). Three configurations of this model are compared to the base-case:

(1) simulation with no explicit calculation of horizontal diffusion (S1),
(2) simulation with zero-gradient temperature BC (S2),
(3) simulation with zero-gradient temperature and wind BC (S3).

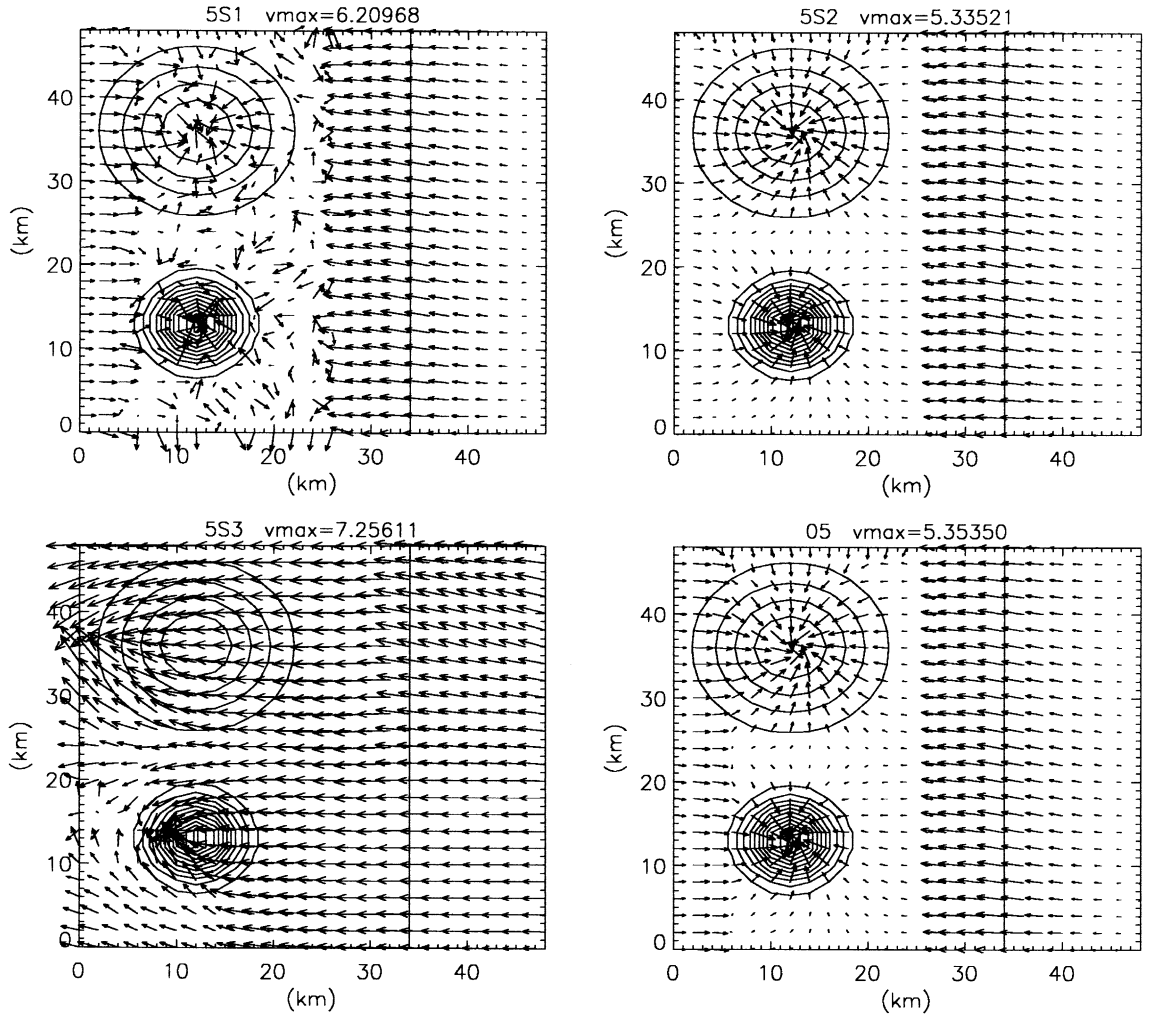

Fig. 16. Same as Fig. 15 at 10:00 LST.

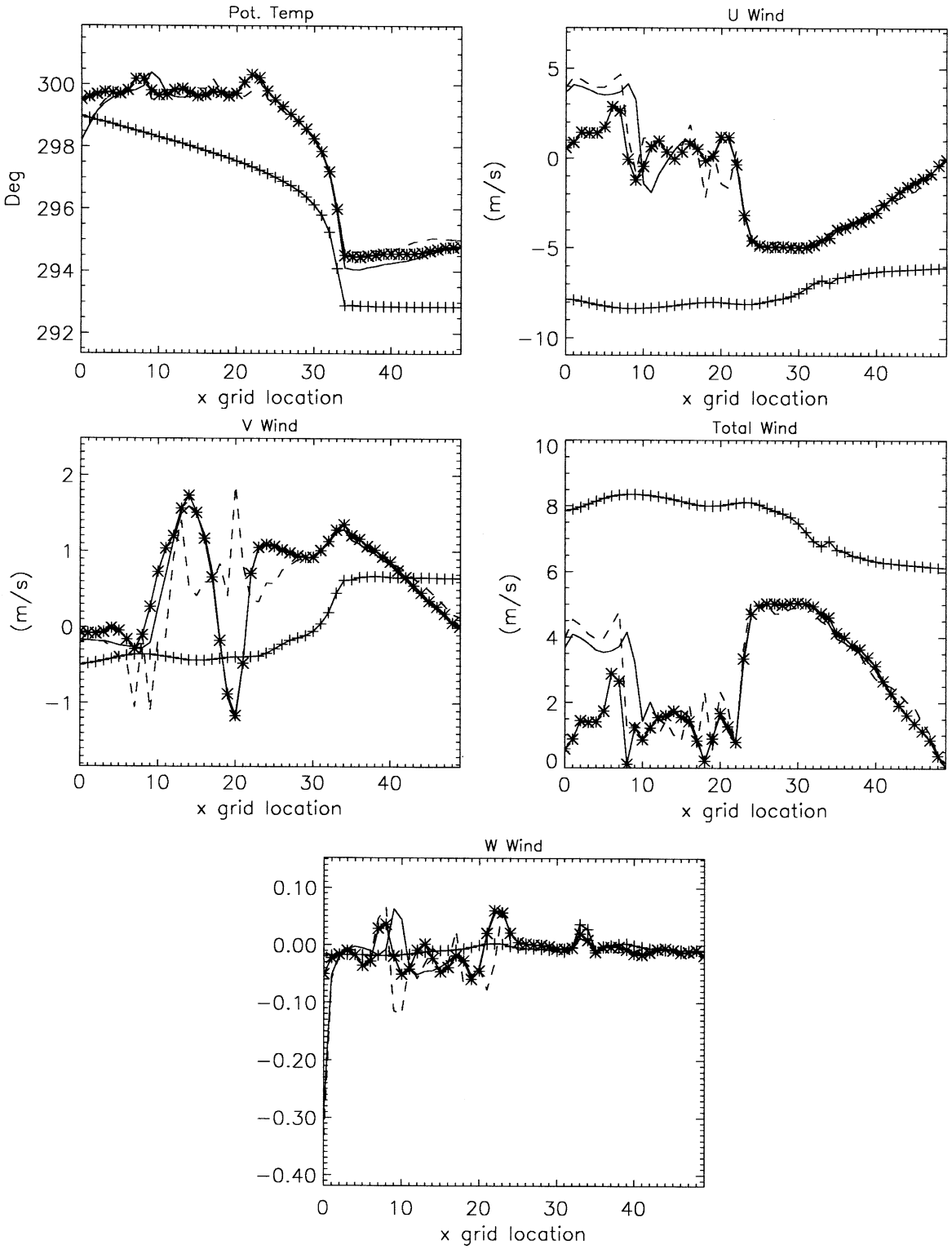

Fig. 17. Comparison of potential temperature, E–W, N–S and vertical wind components on a *XZ* cross-section passing in between the two ridges ($Y = 23$) at 12:00 LST for the four different simulations carried out with Model 05 using different boundary conditions (refer to text and Figs. 15 and 16). The line codes are the following: solid line for base case FVM simulation, dotted line for S1, asterisk-line for S2 and plus-line for S3.

A first look on the results shows the dramatic impact of different boundary conditions. Indeed, the simulation with zero wind and temperature gradients appear to be completely different from the three others, differences starting to become important as soon as the simulation starts (Fig. 15). In this simulation, the zero-gradient condition on wind is the only modification as compared to S2, implying that this condition is the one that generates the largest variability among results. The impact of horizontal diffusion is seen mostly in areas where the forcing is not large enough to generate marked circulations. This is especially true in the area located between the mountains and the sea-breeze front around 1000 LST. At this time, wind fields look chaotic in the non-smoothed results (Fig. 16) and differences in wind intensities reach a factor 3 or 4, the less diffusive simulation producing the stronger winds. Note that these differences are only marked at specific locations and time. As can be seen at 1200 LST on the *xz* profile (Fig. 17), both smoothed and nonsmoothed simulations produce then the same results although smoothed results appear of course less chaotic. The impact of the zero-gradient temperature condition is marked especially during the warming period, i.e. when turbulence is active. Then temperatures advected inside the domain are higher than when the BC are fixed. The contrast with surface temperature is less important and weaker winds are generally observed. Those differences are, however, only seen near the boundaries and disappear in the middle of the domain during daytime and nighttime. The quantitative variability of the model results obtained with a single model is close to the one observed when all models are considered, meaning that the two factors selected in this section are responsible for most of the variability observed in MESOCOM.

7. Conclusions

In most of the mesoscale-model inter-comparison exercises performed to date, measurements were used for model evaluation purposes. As is always the case in such exercises, there is some freedom on the choice of the initial and boundary conditions. Therefore a natural and unavoidable calibration is thus operated in which the competence of the model user becomes a key factor in determining the quality of the model results.

The purpose of MESOCOM is to compare model results only, trying to reduce the influence of the model user to a minimum. An ideal domain has been set up for which a maximum number of initial and boundary conditions were fixed. Seven different modelling groups participated in this study with their respective models. The work presented here has pointed out that even though the case set-up was relatively simple, discrepancies among model results were far from being negligible. Of course, differences in the specification of the assigned initial boundary and initial conditions may result in large differences and this is why part of the inter-comparison work was devoted to check that each model was satisfying those conditions. Despite this, differences in heating and cooling rates in the surface layer were shown to be important and this being especially true over flat terrain. Above hilly terrain, differences were found to be much less important resulting in a more coherent behaviour. Those heating/warming differences resulted in differences in predicted wind fields. Although the prediction of the sea-breeze intensities and locations pointed out some difference (a factor 2 in intensity between the weakest and strongest model predicted wind speed), those differences were much smaller than those obtained in the predicted intensity of the up-slope flows. The inter-comparison has also revealed a few points that needed further investigation, e.g. the larger warming exhibited by some models during the course of the day.

Two factors are thought to be responsible for most of the result variability and were checked quantitatively by using a single model (FVM) in different configurations. These two factors are the horizontal diffusion parameterisation and the inflow boundary conditions for transport. The resulting variability was shown much more important for the second of these factors than for the first one. This was shown to be particularly true from the comparison of zero-gradient wind BC to the case in which zero-gradient BC were imposed to both wind and temperature. The variability obtained between these single model simulations being of the same order of magnitude than the one obtained for the full MESOCOM study, indicating that those two factors are probably responsible for most of the observed variability. It turns out that the definition "in flow" boundary condition corresponds effectively to a variety of implementation in the models and to actually different specifications at the boundaries. Another factor influencing the variability of the model results is the translation of the common surface temperature variability to surface heat fluxes through the surface layer parameterisation schemes. The flow evolution caused by initial differences in the surface heat flux produces even larger differences as time evolves. Such a positive feed-back on the flow evolution is one of the main causes for the differences among the results.

8. Future activities

The topography selected for the study is the result of a compromise between the necessary requirement of simple relations between model results and a few specific parameters with the necessity to reproduce realistic atmospheric circulation for model validation. MESOCOM enabled the identification of some key areas,

which are source of important differences among model results. These areas need further simplifications of the case set-up in order to be interpreted fully. Future exercises will therefore move towards increased simplicity, and among others towards flat terrain or 2-D simulations. Once models are satisfactorily in agreement under these conditions, more complex cases will again be considered. Model results and case description are public domain at http://rem.jrc.cec.eu.int/mesocom.

References

Bartzis, J.G., 1989. Turbulent diffusion modelling for wind flow and dispersion analysis. Atmospheric Environment 23 (9), 1963–1969.

Bartzis, J.G., Venetsanos, A., Varvayanni, M., Catsaros, N., Megaritou, A., 1991. ADREA-I. A transient three dimensional transport code for complex terrain and other application. Nuclear Technology 94, 135–148.

Clappier, A., Perrochet, P., Martilli, A., Muller, F., Krueger, B.C., 1996. A new non-hydrostatic mesoscale model using a Control Volume Finite Element (CVFE), discretisation technique. In: Borrell et al. (Eds.), Proceedings of EUROTRAC Symposium 96, Vol. 1. Southampton, pp. 527–531.

Doyle, J.D., Durran, D.R., Chen, C., Colle, B.A., Georgelin, M., Grubisic, V., Hsu, W.R., Huang, C.Y., Landau, D., Lin, Y.L., Poulos, G.S., Sun, W.Y., Weber, D.B., Wurtele, M.G., Xue, M., 2000. An intercomparison of model predicted wave breaking for the 11 January 1972 Boulder windstorm. Monthly Weather Review 128 (3), 901–914.

Lüpkes, C., Schlünzen, K.H., 1996. Modelling the Arctic convective layer with different turbulence parameterisations. Boundary-Layer Meteorology 79, 107–130.

Oettl, D., 2000. Further development, validation and application of a mesoscale model. Ph.D., University of Graz, Austria, 155pp.

Oettl, D., Almbauer, R.A., Sturm, P.J., Piringer, M., Baumann, K., 2000. Analysing the nocturnal wind field in the city of Graz. Austria. Atmospheric Environment 35, 379–387.

Pielke, R., 1984. Mesoscale Meteorological Modelling. Academic Press, New York, 468pp.

Schayes, G., Thunis, P., Bornstein, R., 1996. Topographic vorticity-mode mesoscale ß (TVM) model: Part I: Formulation. Journal of Applied Meteorology 35, 1815–1823.

Schlünzen, K.H., 1990. Numerical studies on the inland penetrations of sea breeze fronts at a coastline with tidally flooded mudflats. Controlled Atmospheric Physics 63, S.243–256.

Schlünzen, K.H., Bigalke, K., Lüpkes, Ch., Niemeier, U., Von Salzen, K., 1996. Concept and realization of the mesoscale transport- and fluid model METRAS. METRAS Technical Report, 5, Meteorologisches Institut, Universitaet Hamburg, S.145.

Thunis, P., Clappier, A., 2000. Formulation and evaluation of a nonhydrostatic mesoscale vorticity model (TVM). Monthly Weather Review 128 (9), 3236–3251.

Xue, M., Droegemeier, K.K., Wong, V., 2000a. The Advanced Regional Prediction System (ARPS)—a multiscale nonhydrostatic atmospheric simulation and prediction tool. Part I: Model dynamics and verification. Meteorological Atmospheric Physics, submitted for publication.

Xue, M., Droegemeier, K.K., Wong, V., Shapiro, A., Brewster, K., Carr, F., Weber, D., Liu, Y., Wang, D.-H., 2000b. The Advanced Regional Prediction System (ARPS)—a multiscale nonhydrostatic atmospheric simulation and prediction tool. Part II: Model physics and applications. Meteorological Atmospheric Physics, submitted for publication.